Remote Sensing Image Fusion Based On IHS and Dual Tree Compactly Supported Shearlet Transform

Chang Duan[1,2], Qihong Huang[3], Xuegang Wang[1], Shuai Wang and Hong Wang[1]

[1]*School of Electronic Engineering, University of Electronic Science Technology of China*
[2]*Research Institute of Electronic Science and Technology, University of Electronic Science Technology of China*
[3]*Electronic Engineering College, Chengdu University of Information Technology*
Pertinax@163.com;

Abstract

This paper presents a novel remote sensing image fusion algorithm, which implements the intensity-hue-saturation (IHS) transform on panchromatic sharpening of multispectral data and the dual-tree compactly supported shearlet transform (DT CSST) during fusion. Shearlet transforms can provide almost optimal representation of the anisotropic features of an image. The spatial domain discrete implementation, the compactly supported shearlet transform (CSST), which represents the directions by dilation operations, are selected in the proposed fusion method. Since most of the prominent features of images, such as edges and regions, have limited sizes in the spatial domain, CSST is very suitable for image fusion. However, the conventional CSST is shift-variant, which causes distortions in fused images. With the embedded dual-tree (DT) sturcture in the CSST, the shift-variant properties can be effectively reduced. Combining the IHS transform and the DT CSST, an effective panchromatic and multispectral image fusion method is proposed in this paper. The experiments' results suggest that the proposed method extract more spatial information from panchromatic images with less lost in spectral consistency compared to other fusion methods which are based on discrete wavelet transform (DWT), à trous wavelet transform, à trous shearlet transform, the dual-tree complex wave transform (DT CWT), or the Curvelet transform.

Keywords: *Compactly supported shearlet transform, panchromatic multispectral image fusion, Pan-sharpening, Dual-tree*

1. Introduction

Different image sensors are equipped on satellites to capture different images of the same area or object. Generally, there are two types of images recorded on a satellite: pan-chromatic images, which record the total intensity of radiation falling on each pixel, and multispectral images, which record the intensity of radiation in a small band of visible spectra, include the red-green-blue (RGB) region and infrared region. The wavelengths of RGB region are ranging from 0.7 μm to 0.4 μm and the wavelengths of infrared region are ranging from 0.7 μm to 10 μm or greater which are further classified as near infrared (NIR), middle infrared (MIR), or far infrared (FIR or thermal). Panchromatic images supply high spatial resolution for distinguishing features, while multispectral images supply high spectral resolution. In many applications, it would be more helpful if images had both high spatial and high spectral resolutions. This has led to creation of the panchromatic and multispectral image fusion

method or pan-sharpening method, which is very important development in this field of study.

The panchromatic and multispectral image fusion method has been studied for decades. In the early period of this research, the fused images were simply a linear combination of source images, such as Brovery Transform [1]. The early methods are relatively simple and the performances of fused results are low. Gradually, researchers realized that colour information is actually useful and should be maintained. Thus, many solutions in colour space have been proposed, and the representative methods are IHS[2] and principal component analysis (PCA) [3] algorithms, in which a main spectral component is generated from MS-images, and this main component will be substituted by pan-images to increase the spatial resolution prior to inverse IHS or PCA transform. By this procedure, spatial resolution is increased and the spectral information is maintained as much as possible. Finally, researchers realized that both the spatial and spectral consistencies should be maintained simultaneously. With the development of harmonic analysis theory, several multi-scale transform-based methods have been proposed. They include the DWT [3], the analytic wavelet transform (AWT) [4], the dual-tree complex wavelet transform [5, 6], and the curvelet [7, 8]. Many of these methods combine IHS or PCA simultaneously.

Among the multi-scale transforms, the shearlet system stands out in recent years for its efficient representation of multidimensional data. Indeed, many other transforms have been introduced to overcome the limitation of traditional multi-scale methods which cannot capture edges and other anisotropic features in a satisfactory manner. The shearlet transform has many advantages. For example, it is unique in that it has a single or finite set of generating functions; it provides almost optimal representations for multi-dimensional data; It allows a unified treatment of the continuum and digital realms, and it provides a compactly supported transform. Presently, there are two categories of the implementation of the discrete shearlet transform: Frequency-domain based approaches and spatial-domain based approaches. The frequency-domain based approaches have better frequency localization, while the spatial-domain based approaches have better spatial localization. Suppose that the sizes of the frequency and spatial windows are S_F and S_S, respectively. According to the Uncertainly Principle, the product of $S_F \times S_S$ is a constant, meaning that increasing or decreasing both S_F and S_S simultaneously is impossible. In the case of image fusion, spatial localization is more important than frequency localization because most of the salient features of images, such as the regions and edges, have limited sizes in the spatial domain, and the human visual system also extracts that information directly from the spatial domain. The compactly supported shearlet transform (CSST) belongs to the spatial-domain based implementation category [9, 10]. However, CSST has a shift-variant disadvantage to image fusion because it is based on a traditional critically-sampled discrete wavelet transform. Fortunately, this disadvantage can be sophisticatedly mitigated by the dual-tree structure, the details of which will be discussed in Section 3.

Many image fusion methods based on the shearlet transform have been proposed recently. A remote sensing image fusion method based on the band-limited shearlet transform (BLST) has been proposed by[11], and is claimed to be superior to the curvelet method. Miao [12, 13] discussed the multi-focus image fusion method based on the CSST; however, the shift-variant property of the CSST was not considered and consequently, no compensation was made for it. [14] proposed an IHS and shearlet-based pan-MS image fusion method, but did not clearly describe which type of shearlet implementation was used.

In this paper, the dual-tree compactly supported shearlet transform (DT CSST), which is almost shift-invariant, is proposed firstly. Then, a Pan-MS image fusion method based on IHS

and DT CSST is proposed. The IHS guarantees the spectral consistency, and the DT CSST provides the ability to extract more spatial information from the pan-image. The rest of the paper is organized as described in the following sentences. The basic theory of the shearlet transform and its digital implementation of CSST are introduced in Section 2. The construction of DT CSST and its shift invariant property are introduced in Section 3. The proposed remote image fusion method is given in Section 4. After the experiments and analysis in Section 5, a conclusion is drawn in Section 6.

2. Shearlet Transform

In this section, the basic theory of the shearlet transform and the implementations of CSST are briefly introduced.

A shearlet transform is a special case of the composite dilation wavelet transform. The dilation operation D_M is given as:

$$D_M \psi(x) = |\det M|^{-1/2} \psi(M^{-1}x), M \in GL_d(\mathbf{R}),\qquad(2.1)$$

where M is the parameter of the dilation operation, $\psi(x)$ is any function, and $GL_d(\mathbf{R})$ represents the group of d-dimensional invertible matrices defined on $\mathbf{R}$. The translation operation T_t is given as:

$$T_t \psi(x) = \psi(x-t), t \in \mathbf{R}.\qquad(2.2)$$

Let $A_a = \begin{pmatrix} a & 0 \\ 0 & a^{1/2} \end{pmatrix}$, $a > 0$ be the parabolic scaling matrices, and $S_s = \begin{pmatrix} 1 & s \\ 0 & 1 \end{pmatrix}, s \in \mathbf{R}$ be the shearing matrix. The continuous shearlet system $SH(\psi), \psi \in L^2(\mathbf{R}^2)$ is defined by:

$$SH(\psi) = \{\psi_{a,s,t} = T_t D_{A_a} D_s \psi : a > 0, s \in \mathbf{R}, t \in \mathbf{R}^2\}.\qquad(2.3)$$

The definition of the continuous shearlet transform of $f \in L^2(\mathbf{R}^2)$ is the mapping:

$$f \mapsto SH_\psi f(a,s,t) = \langle f, \sigma(a,s,t)\psi \rangle, (a,s,t) \in \mathrm{S},\qquad(2.4)$$

where $\mathrm{S} : (\mathbf{R}^+ \times \mathbf{R}) \times \mathbf{R}^2$, $\sigma(a,s,t)\psi = T_t D_{A_a} D_{S_s} \psi$. The irregular discrete shearlet system upon ψ and Λ is $DSH(\psi, \Lambda) = \{\psi_{a,s,t} = a^{-\frac{3}{4}} \psi(A_a^{-1} S_s^{-1}(\cdot - t)) : (a,s,t) \in \Lambda\}$. A (regular) discrete shearlet system associated with ψ, denoted by $SH(\psi)$, is defined by $SH(\psi) = \{\psi_{j,k,m} = 2^{\frac{3}{4}j} \psi(S_k A_{2^j} \cdot - m) : j,k \in \mathbf{Z}, m \in \mathbf{Z}^2\}$. Notice that the regular versions of discrete shearlet systems are derived from irregular systems by choosing $\Lambda = \{(2^{-j}, -k, S_{-k} A_{2^{-j}} m) : j,k \notin \mathbf{Z}, m \in \mathbf{Z}^2\}$. The discrete shearlet transform of $f \in L^2(\mathbf{R}^2)$ is the mapping defined by:

$$f \mapsto DSH_\psi f(j,k,m) = \langle f, \psi_{j,k,m} \rangle, (j,k,m) \in \mathbf{Z} \times \mathbf{Z} \times \mathbf{Z}^2\qquad(2.5)$$

Cone-adapted shearlets were introduced for the purpose of treating the different directions more equally, so the number of directions could be limited [15].

In the study by Lim [9], the principle and the details of the construction of the CSST were presented, including separable and non-separable transforms. The separable shearlet generator was written as $\varphi(x_1, x_2) = \gamma(x_1)\theta(x_2)$, where the details of γ and θ are given in Corollary III.3 of Lim's study [9]. The forward and backward steps of the CSST are given in Figure 1. The input function $f(x)$ is first processed by the shear

operation along vertical and horizon directions in the spatial domain. Then, the anisotropic discrete wavelet transform (ADWT) is performed on every sheared version of the input image. The outputs of ADWT, $C_{j,1,m}\cdots C_{j,k,m}$ and $\tilde{C}_{j,1,m}\cdots\tilde{C}_{j,k,m}$, are the coefficients of two cones of where j is the scale parameter, k is the number of directions, m refers the positions.
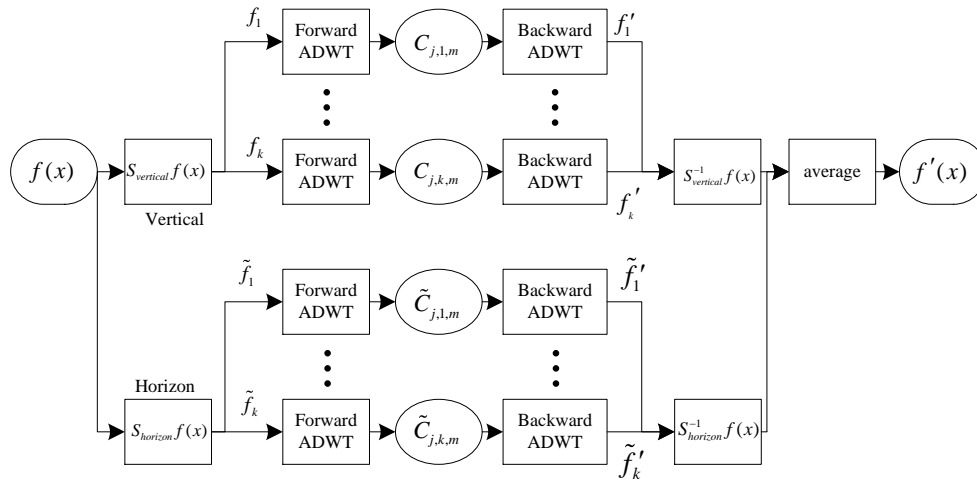

Figure 1. Forward and Backward of CSST

3. Dual-tree Compactly Supported Shearlet Transform

The dual-tree complex [16, 17] wavelet transform employs two real discrete wavelet transforms (DWTs). The first DWT gives the real part of the transform, while the second DWT gives the imaginary part. The two real wavelet transforms use two different sets of filters, each of which satisfies the PR (Perfect Reconstruction) conditions separately. The two sets of filters are jointly designed so that the overall transform is approximately analytic. If these two DWTs satisfy the half-sample delay condition, which also means that the wavelets form an approximate Hilbert transform pair, then the transform would be approximately shift-invariant.

Heuristically, the definitions of forward DT CSST can be represented as follows:

Let $CS_{\psi,\varphi}f(j,k,m)$ represent DT CSST, its coefficients can be calculated by:

$$CS_{\psi,\varphi}f(j,k,m)=SH_{\psi}f(j,k,m)+jSH_{\varphi}f(j,k,m), \tag{3.1}$$

where $SH_{\psi}f(j,k,m)$ and $SH_{\varphi}(j,k,m)$ denote the real and imaginary parts of the complex coefficients, which are calculated by equation (2.4). The backward DT CSST transform or reconstruction of f is given by:

$$\tilde{f}(j,k,m)=\frac{1}{2}\sum_{j,k\in\mathbf{Z},m\in\mathbf{Z}^2}\langle f,\psi_{j,k,m}\rangle\psi_{j,k,m}+\frac{1}{2}\sum_{j,k\in\mathbf{Z},m\in\mathbf{Z}^2}\langle f,\varphi_{j,k,m}\rangle\varphi_{j,k,m} \tag{3.2}$$

This study used the same method as used by [17, 18]. Kingsbury proceeded to illustrate the shift-variance of DWT and the shift-invariance of DT CWT; the comparison of reconstruction results, each single scale-by-scale, for a traditional CSST and DT CSST are given in Figure 2. The input is a white circle located at the centre of a black background. The first and second rows are the reconstruction for the same direction for a horizontal cone of the DT CSST and CSST, and the third and fourth rows are the reconstruction for the same direction for a vertical cone of the DT CSST and

CSST. It was observed in Figure 2(a) that both the CSST and the DT CSST can reconstruct the input image precisely, but in different scales, and that the reconstruction of DT CSST is much smoother than that of CSST. This comparison shows the shift-variant effect of the CSST and the approximate shift-invariant effect of the DT CSST.
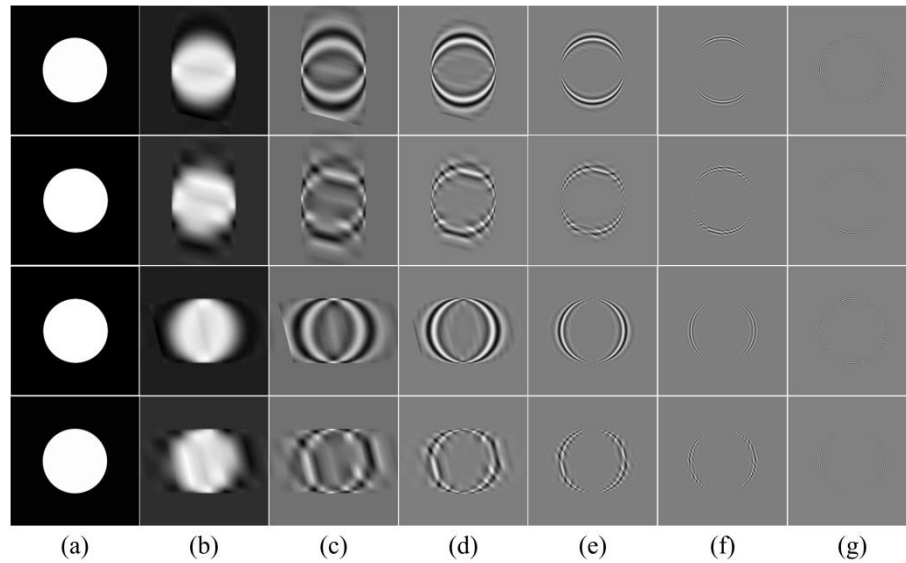

(a)   (b)   (c)   (d)   (e)   (f)   (g)

Figure 2. The Comparison of Reconstruction

(a) the reconstruction of all coefficients, (b) the reconstruction of the low frequency coefficients alone, and (c) to (g) the reconstruction for each different single scale of high frequency coefficients

4. Proposed Method and Measurements
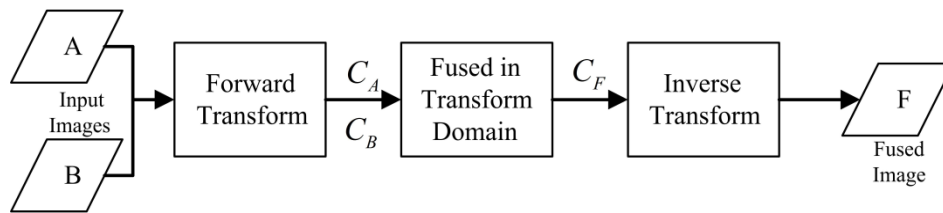
4.1 General Image Fusions

Figure 3. General Image Fusion

General image fusion (GIF), in this paper, refers to steps A and B in Figure 3. A and B represent two input images, and they are decomposed by certain forward transforms into two sets of coefficients, denoted by C_A and C_B. Then, under certain fusion rules, these coefficients are fused into one set, which is denoted by C_F. Finally, an inverse transform is performed and the output image F is the fused image.

The source images C_A and C_B decomposed by DT CSST from source images have different features: C_A is generated from the pan-image, which is monochromic with high spatial resolution and C_B is generated from MS-images, which contain spectral information. In the fusion rule, the high frequency coefficients C_{FH} are extracted from

C_A and the low frequency coefficients C_{FL} are the average of both C_A and C_B as given in:

$$\begin{cases} C_{FL} = mean(C_{AL} + C_{BL}) \\ \quad C_{FH} = C_{AH} \end{cases}. \tag{4.1}$$

After fusion, the fused image contains both spatial and spectral information.

4.2 IHS Transform

The IHS colour transform effectively separates spatial I and spectral H and S information from a standard RGB image. It relates to the human colour perception parameters. The mathematical context is expressed by equation (4.2). I represents the intensity, while 'v_1' and 'v_2' represent intermediate variables which are needed in the transform. H and S stand for hue and saturation (Elghazali 2011).

$$\begin{pmatrix} I \\ v_1 \\ v_2 \end{pmatrix} = \begin{pmatrix} \frac{1}{\sqrt{3}} & \frac{1}{\sqrt{3}} & \frac{1}{\sqrt{3}} \\ \frac{1}{\sqrt{6}} & \frac{1}{\sqrt{6}} & \frac{-2}{\sqrt{6}} \\ \frac{1}{\sqrt{2}} & \frac{-1}{\sqrt{2}} & 0 \end{pmatrix}\begin{pmatrix} R \\ G \\ B \end{pmatrix} \quad \begin{pmatrix} R \\ G \\ B \end{pmatrix} = \begin{pmatrix} \frac{1}{\sqrt{3}} & \frac{1}{\sqrt{6}} & \frac{1}{\sqrt{2}} \\ \frac{1}{\sqrt{3}} & \frac{1}{\sqrt{6}} & \frac{-1}{\sqrt{2}} \\ \frac{1}{\sqrt{3}} & \frac{-2}{\sqrt{6}} & 0 \end{pmatrix}\begin{pmatrix} I \\ v_1 \\ v_2 \end{pmatrix}$$

$$H = \tan^{-1}\left(\frac{v_2}{v_1}\right) \tag{4.2}$$

$$S = \sqrt{v_1^2 + v_2^2}$$
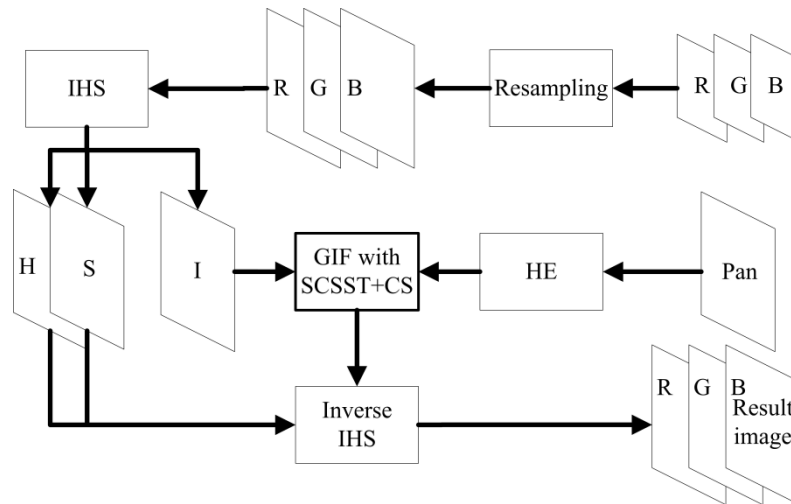
4.3 IHS Combined with GIF based on DT CSST

Figure 4. Steps of the Proposed Algorithm

The steps of the proposed method are given in Figure 4. In the first step, the source images are registered. Then, the small-sized MS-images are resized to the same size as the pan-image, and the IHS transform is performed on the resized MS-images; the output are the I, H, and S components. Next, the histogram equalization (HE) operation is performed on the pan-image, according to the grey-scale distribution of the I-component of the multispectral images, this step can make the substituted I-component of the pan-image closer to that of the MS-images, which can retain the

spectral consistency. GIF based on the DT CSST is performed in the next step. Finally, the inverse IHS transform is performed, and the result is the final fused image.

4.4 Performance Measurements

Two measurement groups were utilized to analyze the performance; one is related to the space consistency where mutual information (MI), $Q^{AB|F}$ of [18] and $Q0$ of [19] are the selected performance indices, and the other type is related to spectral consistency, where $RASE$, $ERGAS$ and $Q3$ of [2] are the selected performance indices.

MI measures how much information, which originated in the source images, is contained in the fused image. It is defined as:

$$MI = I_{FA} + I_{FB},\qquad(4.3)$$

where $I_{FA}(f,a)=\sum_{f,a}P_{FA}(f,a)\log\dfrac{P_{FA}(f,a)}{P_F(f)P_A(a)}$, $I_{FB}(f,b)=\sum_{f,b}P_{FB}(f,b)\log\dfrac{P_{FB}(f,b)}{P_F(f)P_B(b)}$, and P is the distribution of grey-scale of images.

$Q^{AB|F}$ in the study by[2] evaluates the amount of edge information that is transferred from the input images to the output fused images. The larger the $Q^{AB|F}$, the more amount of important edge information is being transferred.

$Q0$ of [20] is defined as:

$$Q0 = \frac{4\sigma_{xy}\overline{xy}}{(\overline{x}^2+\overline{y}^2)(\sigma_x^2+\sigma_y^2)} = \frac{\sigma_{xy}}{\sigma_x\sigma_y}\cdot\frac{2\overline{xy}}{\overline{x}^2+\overline{y}^2}\cdot\frac{2\sigma_x\sigma_y}{\sigma_x^2+\sigma_y^2},\qquad(4.4)$$

where x and y denote two input images, $\overline{x}$ and $\overline{y}$ are the mean of x and y, and σ_x^2 and σ_{xy} denote the variance of x and the covariance of x, y. The value of $Q0$ is between -1 and 1. The maximum value of 1 is achieved when x and y are identical.

$RASE$ is defined as (4.5), can estimate the average performance of the method of image fusion in the spectral bands.

$$RASE = \frac{100}{M}\sqrt{\frac{1}{N}\sum_{i=1}^{N}RMSE^2(S_i)},\qquad(4.5)$$

where M is the mean radiance of N spectral images (S_i) of the original MS bands, RMSE is the root mean square error defined as: $RMSE^2(S_i)=bias^2(S_i)+SD^2(S_i)$.

$ERGAS$ refers to the relative global dimensional synthesis error as in euqtion (4.6):

$$ERGAS = 100\frac{h}{l}\sqrt{\frac{1}{N}\sum_{i=1}^{N}\frac{RMSE^2(S_i)}{M_i^2}},\qquad(4.6)$$

where h is the resolution of the pan-image, l is the resolution of the MS-images, and M_i is the mean radiance of each spectral band. The lower the value of RASE and the ERGAS indexes, the higher the spectral quality of the fused images.

For the original MS-images with three spectral bands, let a_1, b_1, and c_1 denote the radiance value of a given image pixel in the fourth band. For the fusion images with three spectral bands, let a_2, b_2, and c_2 denote the radiance values of a given image pixel in the four bands. Let $z_1 = a_1 + ib_1 + jc_1$ and $z_2 = a_2 + ib_2 + jc_2$ denote the three-band original MS image and the fusion product, respectively, both of which are expressed as quaternion. Then, $Q3$ is defined as in Equation (4.7).

$$Q3 = \frac{\left|\sigma_{z_1 z_2}\right|}{\sigma_{z_1} \cdot \sigma_{z_2}} \cdot \frac{2\sigma_{z_1} \cdot \sigma_{z_2}}{\sigma_{z_1}^2 + \sigma_{z_2}^2} \cdot \frac{2\left|\overline{z}_1\right| \cdot \left|\overline{z}_2\right|}{\left|\overline{z}_1\right|^2 + \left|\overline{z}_2\right|^2} , \qquad (4.7)$$

where $\sigma_{z_1 z_2}$ is the hyper-complex covariance between z_1 and z_2, σ_{z_1} and σ_{z_2} are the square roots of the variances of z_1 and z_2, $\overline{z}_1$ and $\overline{z}_2$ are the expected values of z_1 and z_2, and $|\bullet|$ is the modulus of $\bullet$. $Q3$, in fact, is the vector version of $Q0$. The maximum value of 1 is achieved when z_1 and z_2 are identical.
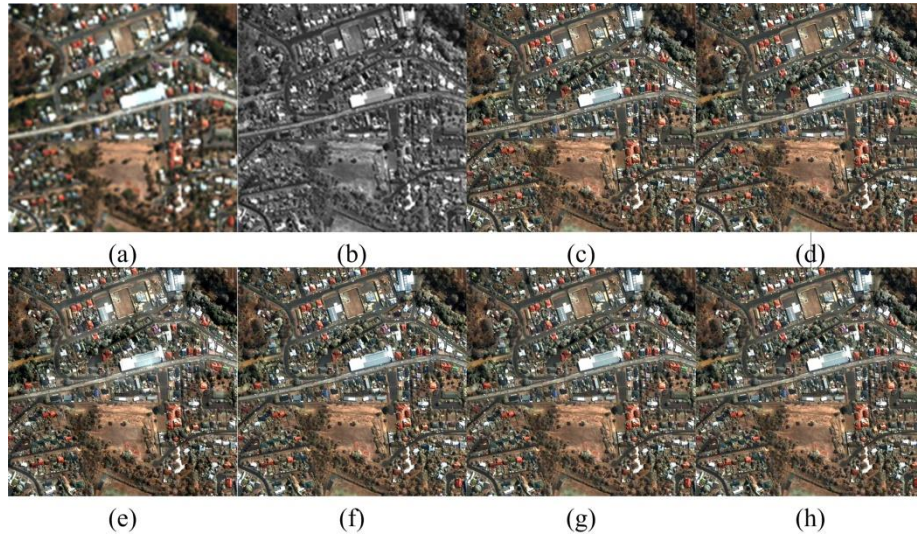
5. Experiments and Analysis

Figure 5. Source and Result Images of the First Group

(a) Multispectral images, (b) Panchromatic image, (c) fused image by DT CSST, (d) fused image by curvelet, (e) fused image by DWT, (f) fused image by DTCWT, (g) fused image by à trous wavelet, (h) fused image by à trous shearlet

In this section, the results of experiments performed to evaluate the qualities of the proposed method are reported. Three groups of data are used as the source data, where the first and second groups are originated from IKONOS, and third group is originated from QuickBird. The spatial resolution of IKONOS is 1 m for the panchromatic image and 4 m for the multispectral images. The spatial resolution of QuickBird is 0.6 m for the panchromatic image and 2.4 m for the multispectral images. The sizes of all of the panchromatic images are 512×512; whereas the multispectral images are 128×128. The sources images are shown in (a) and (b) from Figure 5 to Figure 7, where (a) are the multispectral images and (b) are the panchromatic images, and the multispectral images are resized to the same size of panchromatic images.

The result images of three groups of proposed method (c) and other methods based on else transforms combined with IHS (d) to (h) are shown in Figure 7 respectively, where the number of scale equal to five. The visual effect of all of the result images are almost identical, which means that the proposed method, as well as other methods, can effectively extract the spatial information from panchromatic images and combine it with spectral information from

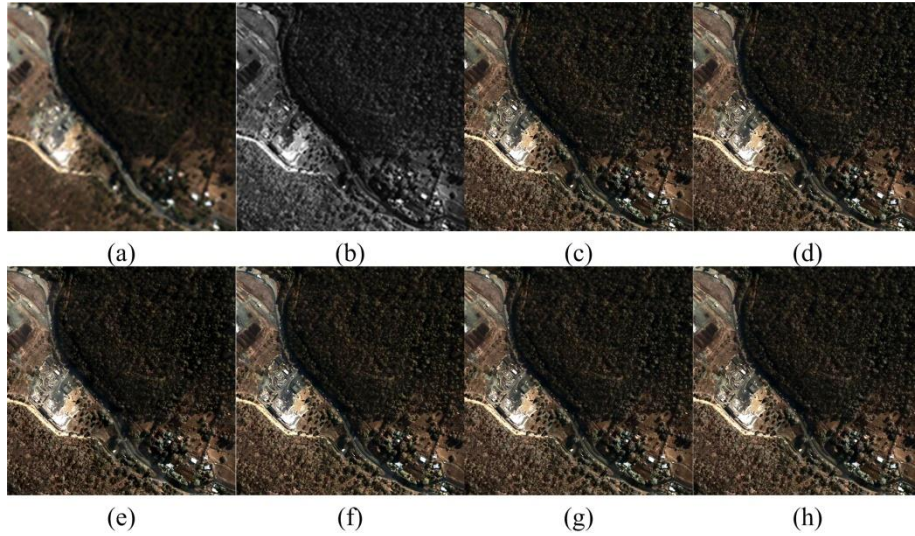the multispectral images, and that the performance cannot really be evaluated simply from the visual effect.

Figure 6. Source and Result Images of the Second Group

(a) Multispectral images, (b) Panchromatic image, (c) fused image by DT CSST, (d) fused image by curvelet, (e) fused image by DWT, (f) fused image by DTCWT, (g) fused image by à trous wavelet, (h) fused image by à trous shearlet
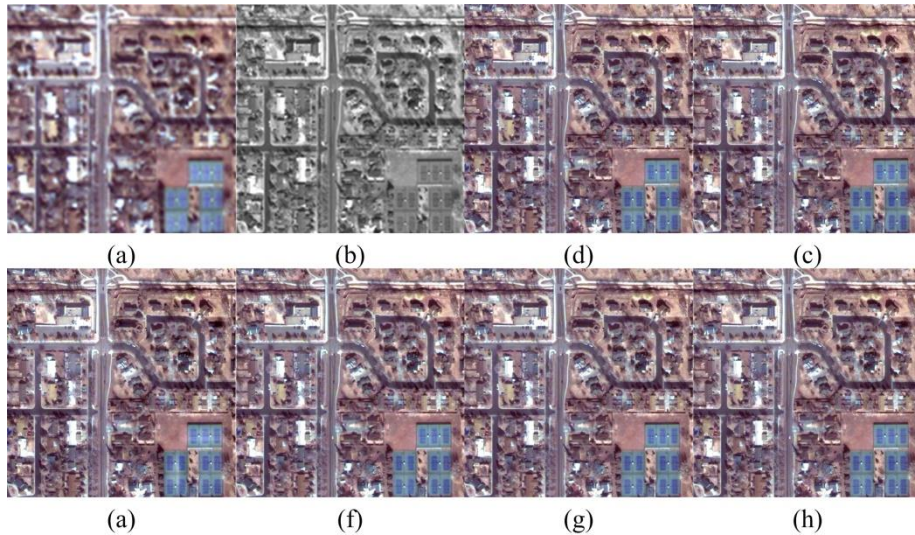

Figure 7. Source and Resulting Images of the Third Group

(a) Multispectral images, (b) Panchromatic image, (c) fused image by DT CSST, (d) fused image by curvelet, (e) fused image by DWT, (f) fused image by DTCWT, (g) fused image by à trous wavelet, (h) fused image by à trous shearlet

When evaluating the performance of all of the methods, both spatial and spectral information need to be take into account, because these two types of measurements are, in fact, negatively correlated, which means that, for certain chosen method, it is impossible to

increase both spatial and spectral consistency simultaneously. Different number of scale provides different proportions of mixture for spatial and spectral information. Usually, if the number of scale is too small, equalling 1 or 2, excessive spectral information will be included in fused images, which ultimately cause many unpleasant regions in fused images. While if the number of scale is too large, over 5 for example, in several implementations of transforms, such as à trous wavelet, à trous shearlet, the size of filter becomes larger than the data which causes inner errors and the methods become useless; and for other transforms, such as DWT, DTCWT, CSST etc. larger number of scale means larger computation cost. Therefore, the recommended numbers of scale are 3, 4 and 5.

Table 1. The Spatial Consistency Performance Indices for Third Group Data

Scale Number		DWT	DTCWT	À trous wavelet	À trous shearlet	Cuvelet	CSST
2	MI	2.7865	3.2022	3.2154	3.1703	3.212	3.2217
	$Q^{AB/F}$	0.42584	0.60288	0.61502	0.61359	0.61001	0.61766
	$Q0$	0.83832	0.95673	0.95868	0.96089	0.95774	0.95887
3	MI	2.6526	3.2341	3.2531	3.244	3.2449	3.2586
	$Q^{AB/F}$	0.56044	0.6533	0.65873	0.65935	0.65633	0.65819
	$Q0$	0.88436	0.96902	0.97023	0.97111	0.96962	0.97031
4	MI	2.6439	3.354	3.3876	3.3892	3.3732	3.3987
	$Q^{AB/F}$	0.62359	0.67546	0.6781	0.67942	0.67689	0.67824
	$Q0$	0.91677	0.97768	0.97889	0.9803	0.97828	0.97923
5	MI	2.7487	3.5589	3.6018	3.6633	3.5822	3.6301
	$Q^{AB/F}$	0.6642	0.68782	0.68869	0.68917	0.68848	0.68858
	$Q0$	0.94641	0.98559	0.98647	0.98795	0.98607	0.98697

Table 2. The Spectral Consistency Performance Indices for Third Group Data

Scale Number		DWT	DTCWT	À trous wavelet	À trous shearlet	Curvelet	CSST
2	$Rase$	11.1636	14.3793	14.611	15.4422	14.4656	14.5817
	$Ergas$	86.8722	111.8956	113.6989	120.1671	112.5673	113.4709
	$Q3$	0.94944	0.91012	0.9075	0.89768	0.90916	0.90785
3	$Rase$	14.5059	16.8123	16.9493	17.327	16.8587	16.8864
	$Ergas$	112.8813	130.8291	131.8948	134.8344	131.1895	131.4051
	$Q3$	0.91756	0.88113	0.87934	0.87449	0.8805	0.88011
4	$Rase$	17.0354	18.3477	18.4794	19.0217	18.3921	18.4686
	$Ergas$	132.565	142.7767	143.8017	148.0214	143.1225	143.7174
	$Q3$	0.88619	0.85953	0.85745	0.84924	0.85881	0.85757
5	$Rase$	19.1829	19.9046	20.0039	20.4483	19.9445	19.9859
	$Ergas$	149.2758	154.8922	155.665	159.1231	155.2026	155.5245

Parts of the performance indices of the third group, with number of scale from 2 to 5, are shown in Table 1 and Table 2. From these two tables, it can be noticed that the à trous shearlet based method has most of the largest values in spatial indices, but its spectral indices are not the best. It's also hard to compare the performances by the values directly. But after the curves, whose first dimension is the spatial indices and the second dimension is the spectral indices, are drawn as shown in Figure 8, the performance can be compared easily. In Figure 8, only the curves of *MI* with *RASE* and *Q3* are shown. In fact, other curves such as *Q0* with *RASE* or $Q^{AB/F}$ with *Q3* etc. are similar to those in Figure 8; therefore they are

ignored for the limitation of the paper. From the curves in Figure 8, it can be noticed in the centre parts of the curves, if a horizontal line is drawn from left to right, it will intersect with all the curves. The curve of proposed method is the last one which the horizontal line intersects with. This suggests that under the case of equal indices for spectral consistency, the proposed method has the largest spatial consistency. And similarly, if a vertically line is drawn, the proposed method has the least *RASE* and highest *Q3*. This also suggests that under the case of equal indices for spatial consistency, the proposed method has the best spectral consistency. To sum up, the results of experiment suggest that the proposed, CSST with IHS based, panchromatic and spectral image fusion method is superior to methods based on other multi-scale transforms such as DWT, DTCWT, à trous wavelet, à trous shearlet or curvelet.
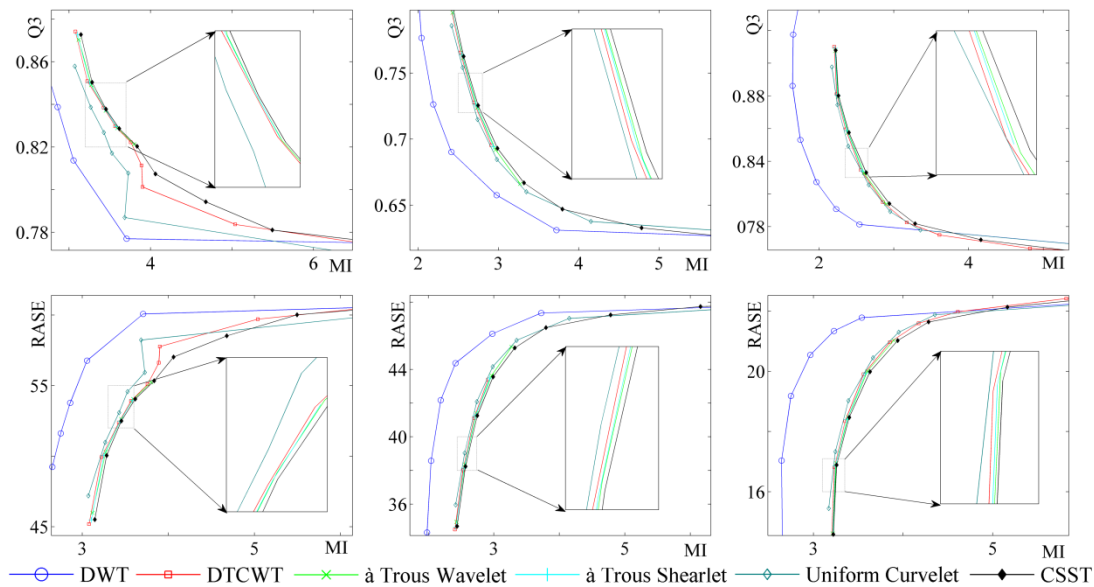

Figure 8. Performance Curves between Spatial and Spectral Consistency

6. Conclusion

Shearlet theory has a better ability to represent anisotropic features of multi-dimensional data than conventional wavelet theory, and the digital implementation of CSST is efficient and effective. The advantages of CSST, such as multi-resolution on directions, compactly supported in the spatial domain, make it very suitable for remote image fusion. However, its shift-variant property leads to distortions in fused images and hampers the performance. The dual-tree structure of DT CWT can be embedded here to reduce the shift variant property of conventional CSST. Combining the DT CSST and IHS transforms, the proposed remote image fusion method can effectively fulfill the task of fusing the panchromatic and the multispectral images. According to the experimental results, the proposed remote image fusion method is superior to the methods based on DWT, à trous shearlet, à trous wavelet, DT CWT, and curvelet transform.

References

[1] E. S. Elghazali, "Performance of Quickbird Image and Lidar Data Fusion for 2d/3d City Mapping," Australian Journal of Basic and Applied Sciences, vol. 5, **(2011)**, pp. 1588-1600**.**

[2] M. Choi, "A new intensity-hue-saturation fusion approach to image fusion with a tradeoff parameter," Geo science and Remote Sensing, IEEE Transactions on, vol. 44, **(2006),** pp. 1672-1682.

[3] M. González-Audícana, J. L. Saleta, R. G. Catalán and R. García, "Fusion of multispectral and panchromatic images using improved IHS and PCA mergers based on wavelet decomposition," Geo science and Remote Sensing, IEEE Transactions on, vol. 42, **(2004),** pp. 1291-1299.

[4] J. Nunez, X. Otazu, O. Fors, A. Prades, V. Pala and R. Arbiol, "Multi resolution-based image fusion with additive wavelet decomposition," Geo science and Remote Sensing, IEEE Transactions on, vol. 37, **(1999),** pp. 1204-1211.

[5] S. Ioannidou and V. Karathanassi, "Investigation of the dual-tree complex and shift-invariant discrete wavelet transforms on Quickbird image fusion," Geo science and Remote Sensing Letters, IEEE, vol. 4, **(2007),** pp. 166-170.

[6] P. R. Hill, D. R. Bull and C. N. Canagarajah, "Image fusion using a new framework for complex wavelet transforms," in Image Processing, 2005. ICIP 2005, IEEE International Conference on, **(2005)**, pp. II-1338-41.

[7] M. Choi, R. Y. Kim, M. R. Nam and H. O. Kim, "Fusion of multispectral and panchromatic satellite images using the curvelet transform," Geo science and Remote Sensing Letters, IEEE, vol. 2, **(2005),** pp. 136-140.

[8] Q. Zhang and B.-l. GUO, "Fusion of remote sensing images based on the second generation curvelet transform," Optics and Precision Engineering, vol. 7, **(2007),** pp. 1131-1135.

[9] W. Q. Lim, "The discrete shearlet transform: a new directional transform and compactly supported shearlet frames," IEEE Trans Image Process, vol. 19, **(2010)** May, pp. 1166-80.

[10] G. Kutyniok and W.-Q. Lim, "Compactly supported shearlets are optimally sparse," Journal of Approximation Theory, vol. 163, **(2011),** pp. 1564-1589.

[11] Y. Chai, Y. He and C. Qu, "Remote sensing image fusion based on iterative discrete Shearlet transform," Computer Engineering and Applications, vol. 47, **(2011),** pp. 174-176.

[12] Q. G. Miao, C. Shi, P. F. Xu, M. Yang and Y. B. Shi, "A novel algorithm of image fusion using shearlets," Optics Communications, vol. 284, **(2011),** pp. 1540-1547.

[13] Q. Miao, C. Shi, P. Xu, M. Yang and Y. Shi, "Multi-focus image fusion algorithm based on shearlets," Chinese Optics Letters, vol. 9, **(2011),** pp. 041001.

[14] C. Deng, S. Wang and X. Chen, "Remote Sensing Images Fusion Algorithm Based on Shearlet Transform," in Environmental Science and Information Application Technology, 2009, International Conference on, **(2009)**, pp. 451-454.

[15] G. R. Easley and D. Labate, "Critically sampled wavelets with composite dilations," Image Processing, IEEE Transactions on, vol. 21, **(2012),** pp. 550-561.

[16] N. Kingsbury, "Complex wavelets for shift invariant analysis and filtering of signals," Applied and computational harmonic analysis, vol. 10, **(2001),** pp. 234-253.

[17] N. Kingsbury, "Image processing with complex wavelets," Philosophical Transactions of the Royal Society of London. Series A: Mathematical, Physical and Engineering Sciences, vol. 357, **(1999),** pp. 2543-2560.

[18] V. Petrovi and C. Xydeas, "On the effects of sensor noise in pixel-level image fusion performance," in Information Fusion, 2000. FUSION 2000. Proceedings of the Third International Conference on, vol. 2, **(2000)**, pp. WEC3/14-WEC3/19.

[19] G. Piella and H. Heijmans, "A new quality metric for image fusion," in Image Processing, 2003. ICIP 2003. Proceedings 2003 International Conference on, vol. 2, **(2003)**, pp. III-173-6.

[20] Z. Wang and A. C. Bovik, "A universal image quality index," Signal Processing Letters, IEEE, vol. 9, **(2002),** pp. 81-84.

Authors

Chang Duan, he received his B.S. and Master degree in school of electronic engineering of University of Electronic Science and Technology of China (UESTC) in 2006 and 2002 respectively. He is currently a phd student of School of electronic engineering of UESTC and work in Research Institute of Electronic Science and Technology of UESTC. His research interests are focused on image fusion, image processing, image compression, *etc.*

Qihong Huang, he received his Master and B.S. Degree in the School of Electronic Engineering from Chongqing University of Posts and Telecommunications (CUPT) in 2000, and in 1997. And he received his Ph.D. degree in electrical engineering from University of Electronic Science and Technology of China (UESTC), His current research interests are focused on image processing and pattern recognition.

Xuegang Wang Gang, he received his Ph.D. in 1992. And currently he is the professor and Ph.D. supervisor of University of Electronic Science and Technology of China (UESTC). His current research interests include radar system and radar signal processing.

Shuai Wang, he received his Master and B.S. Degree in the School of Electronic Engineering from University of Electronic Science & Technology of China in 2004, and in 2001, respectively. He is currently a Lecturer in the School of Electronic Engineering in UESTC. His current research interests are focused on medical image processing, pattern recognition and image fusion.

Hong Wang, he received the B.S. degree in mechanical engineering from Northwestern Polytechnic University, Xi'an in 1996, the M.S. degree in electrical engineering from Chongqing University, Chongqing, in 2003 and the Ph.D. degree in electrical engineering from University of Electronic Science and Technology of China (UESTC), Chengdu, in 2007. His present areas of interest include signal processing and digital communication system.